Draft version August 14, 2020
Typeset using LaTeX twocolumn style in AASTeX63

Magnetic energy balance in the quiet Sun on supergranular spatial and temporal scales

Fabio Giannattasio,[1] Giuseppe Consolini,[2] Francesco Berrilli,[3] and Dario Del Moro[3]

[1] Istituto Nazionale di Geofisica e Vulcanologia, Via di Vigna Murata 605, 00143 Roma, Italy
[2] INAF - Istituto di Astrofisica e Planetologia Spaziali, Via del Fosso del Cavaliere 100, 00133 Roma, Italy
[3] Department of Physics, University of Rome Tor Vergata, Via della Ricerca Scientifica 1, 00133 Roma, Italy

(Received August 14, 2020; Revised; Accepted)

Submitted to ApJ

ABSTRACT

Ubiquitous small-scale magnetic fields (magnetic elements, MEs) in the quiet solar photosphere may play a key role in the storage of magnetic energy and its transfer to the upper atmospheric layers. By invoking the Poynting's theorem it is possible to estimate the rate of change of magnetic energy density in a photospheric plasma volume, once provided the magnetic field, **B**, the electric field, **E**, and the current density, **J**. By taking advantage of a 24-hr long magnetogram time series without interruption acquired by the *Hinode* mission, we computed, for the first time, the average rate of change of magnetic energy density on supergranular spatial and temporal scales. We found that the regions where this quantity is positive correspond with the longest magnetic field decorrelation times, being the latter consistent with the timescales of magnetic energy density variation. This suggests that, on average, the energy provided by photospheric electric and magnetic fields and current density is effective in sustaining the magnetic fields in the network.

Keywords: quiet Sun – Photosphere – Supergranulation

1. INTRODUCTION

The study of the mechanisms responsible for the storage of energy in the solar photosphere and its transport to the upper atmospheric layers is of uttermost importance in active regions as well as in the quiet Sun, where they may trigger a chain of phenomena relevant for Space Weather. In this framework, a substantial contribution to the energy budget of the photosphere is carried by ubiquitous small-scale magnetic fields (magnetic elements, MEs) with characteristic size of the order of - and smaller than - the spatial resolution (about 100 km) achievable by current instruments (see, e.g., Trujillo Bueno et al. 2004; Bellot Rubio & Orozco Suárez 2019). Several studies in the literature have pointed out the key role played by MEs in storing energy in the quiet Sun and their capability to transfer it upward via, for instance, magnetic reconnections (see, e.g., Chae 1999; Viticchié et al. 2006; Rouppe van der Voort et al. 2016; Gošić et al. 2018; Bellot Rubio & Orozco Suárez 2019, and references therein) and/or magnetohydrodynamic waves (see, e.g., Hahn & Savin 2014; Stangalini et al. 2015; Jefferies et al. 2019; Rajaguru et al. 2019, and references therein). However, the processes by which MEs emerge, evolve and organize in the quiet photosphere are still not completely clear, despite the recent efforts aimed to characterize their dynamics on a wide range of spatial and temporal scales, from granular to supergranular (see, e.g., Giannattasio et al. 2013, 2014b,a; Abramenko 2017; Giannattasio et al. 2018; Bellot Rubio & Orozco Suárez 2019; Giannattasio et al. 2019, and references therein).

In order to correctly estimate the amount of available energy in a given photospheric region it is necessary to know the electric field, **E**, and the current density, **J**, as well as the magnetic field, **B**. In fact, all these quantities allow to compute, for example, the Poynting flux, the magnetic helicity (see, e.g., Démoulin & Berger 2003; Schuck 2006; Kazachenko et al. 2014, 2015) and study the evolution of currents and their coupling with electric and magnetic fields. In particular, the variation of the

Corresponding author: Fabio Giannattasio
fabio.giannattasio@ingv.it

magnetic energy content in a volume of photospheric plasma is linked to the work done by the field forces on a distribution of charges via the Poynting's theorem, which states that the rate of variation of the energy density equals the work done by the electric field plus the net rate of energy flux escaping the plasma volume element. More in detail, the rate of work done on the surrounding plasma is expressed via the dot product, $\mathbf{J} \cdot \mathbf{E}$, while the energy flux is described by the divergence of the Poynting vector, **S**. Thus, the interaction between **E**, **J** and **B** plays a fundamental role in the energy balance of the photospheric plasma.

While the computation of the current density does not present criticalities once provided the vector magnetic field, and can be attained by invoking the Ampere's law, the computation of electric field is not trivial and has some aspects to pay attention to. Mainly two techniques have been used in the past to compute the electric field: the spectroscopy observation of the Stark effect (Wien 1916; Davis 1977; Jordan et al. 1980) and the use of the Ohm's law in the ideal MHD regime. While the former method was recognized to be critically affected by the low sensitivity of observations (Moran & Foukal 1991); the latter was improved by considering the component of the Faraday's equation orthogonal to the magnetic field so to obtain both velocity and electric field vectors (Kusano et al. 2002; Welsch et al. 2004; Chae & Sakurai 2008). Various refined techniques have been developed to compute the electric field based on the Faraday's law mixed with observational constraints (see, e.g., Fisher et al. 2010; Kazachenko et al. 2014). These methods are as accurate as complex, and require in input vector magnetograms or full-Stokes data to perform spectropolarimetric inversions via suitable numerical procedures. These requirements imply the acceptance of trade-offs in observations, as it is at present time still not possible to take advantage of robust vector magnetograms (or full-Stokes data to be successfully inverted) at very high spatial resolution and at the same time cover a wide range of both spatial and temporal scales (from granular to at least supergranular scales). However, when dealing with observations targeted at the quiet Sun a reasonable approximation for the photospheric electric field can be still obtained also having only Line of Sight (LoS) magnetograms instead of full vector magnetograms as inputs when averaging over the longest time scales available (let's say of the order of typical time scale of supergranulation). In this case the computation of electric field is much simplified while, in contrast, none of the accurate methods mentioned above is applicable to compute such a "zeroth order" photospheric electric field.

As far as we know, the average properties of photospheric electric field and current density in the quiet Sun on supergranular spatial and temporal scales are still not- or poorly- investigated, although they may play a crucial role in the storage and dissipation of energy in the quiet photosphere. In this work, for the first time we provide an average zeroth-order description of the properties of both the photospheric electric field and current density in the quiet Sun on supergranular scales and their connection with the magnetic energy budget of the photosphere. We take advantage of an unprecedented data set consisting of a $\sim$ 24 hr-long magnetogram time series with high spatial resolution ($\simeq$ 0".3) targeted at the disk center and enclosing an entire supergranule, whose linear size is about $\sim$ 50". The results obtained are discussed in the light of recent studies in literature and may help to shed light on the mechanisms that cause the variation of magnetic energy in the quiet photosphere. The paper is organised as follows. In §2 we describe the data set used and the approach by which the physical quantities averaged on supergranular scales are computed. §3 is devoted to the description of results and their discussion in the light of the previous literature; while in §4 we summarize our findings and drive to conclusions.

2. DATA AND METHODS

2.1. *The data set*

The data analyzed in this work were acquired by the Hinode mission (Kosugi et al. 2007) on 2010 November 2, and are part of the Hinode Operation Plan 151 entitled "Flux replacement in the photospheric network and internetwork". They consist of a magnetogram times series with 90s cadence starting at 08:00:42 UT, lasting for $\sim$ 24 hr without interruption, and targeted at a quiet Sun region in the disk center. Magnetograms were produced by using the spectral line Na I D at 589.6 nm, observed with the Narrowband Filter Imager (Tsuneta et al. 2008) at two wavelengths at $\pm$160 mÅ from the line center. Data were 2×2 binned to a pixel size of $0''.16$, corresponding to $\simeq$ 116 km in the solar photosphere, and a spatial resolution of $\simeq 0''.3$. The magneotogram noise is $\sigma \simeq 4$ G for single magnetograms, and was computed as the rms of the signal in a sub-Field of View (sub-FoV) free of magnetic field convolved with a 3×3 Gaussian kernel. Magnetograms were co-aligned, trimmed to the same FoV, which is $\simeq 51 \times 53$ Mm^2 wide (corresponding to 440×455 pixels^2), and filtered out for five minutes oscillations. Further details can be found in Gošić et al. (2014, 2016).

2.2. *Photospheric electric field, current density, and the Poynting theorem*

In order to compute the plasma horizontal velocity field in the FoV, we applied the Fast Local Correlation Tracking technique (FLCT, Fisher & Welsch 2007, 2008) with a spatial window of ~ 1 Mm (10 pixels) to the filtergram time series simultaneous and co-spatial with the magnetogram time series. This method was proved to be very accurate in retrieving the horizonthal velocity field when the magnetic field is purely vertical (Schuck 2008). The latter hypothesis will be discussed below and in §3. FLCT and its predecessor (the Local Correlation Tracking, LCT) were successfully applied in several works on the same data set, and allowed to obtain results reliable and consistent with previous observations and models (Orozco Suárez et al. 2012; Gošić et al. 2014; Giannattasio et al. 2014b; Requerey et al. 2018; Chian et al. 2019). In particular, Orozco Suárez et al. (2012) showed that the horizontal velocities obtained in the same FoV with the FLCT technique originate radial velocity profiles within the supergranule that are well fitted by the supergranular kinematic model in Simon & Weiss (1989); Simon et al. (2001). The magnetogram and horizontal velocity time series were then averaged to recover the mean vertical magnetic- and horizontal velocity- fields over ~ 24 hr, which is comparable with the temporal scales characteristic of supergranulation (Rast 2003; Del Moro et al. 2004). In Figure 1 we show the mean magnetogram averaged over the whole period of observation, T) of the FoV saturated between -300 and 100 G. The boundaries of a supergranular cell are clearly visible as magnetic field enhancements. The green arrows represent the mean horizontal velocity field as computed with the FLCT method (see also Figure 1a in Giannattasio et al. 2014b).

In the ideal case of very high magnetic Reynolds numbers such those in the solar photosphere (see, e.g., Parker 1963; Weiss 2001; Hirzberger 2002; Cattaneo et al. 2003; Hood & Hughes 2011; Rieutord et al. 2012) the conductivity diverges, and for the Ohm's law a finite current density, $\mathbf{J}$, is possible only if

$$\frac{\mathbf{J}}{\sigma} = \mathbf{E} + \frac{\mathbf{v}}{c} \times \mathbf{B} = 0 \Rightarrow \mathbf{E} = -\frac{\mathbf{v}}{c} \times \mathbf{B}, \tag{1}$$

where $\mathbf{E}$, $\mathbf{B}$, and $\mathbf{v}$ are the electric field, the magnetic field and the plasma velocity, respectively, and we have adopted cgs-Gaussian units. Let us consider the following geometry: the versor $\hat{\mathbf{z}}$ points upward along the direction perpendicular to the photosphere, $\hat{\mathbf{y}}$ lays on the photospheric plane and is directed toward the solar North, and $\hat{\mathbf{x}}$ completes the orthonormal triad toward the solar East. If we assume that the magnetic field averaged on supergranular time scales T is mainly vertical at photospheric heights (see the discussion in the next section) and in potential configuration (null helicity), namely $\langle \mathbf{B} \rangle_T \simeq \langle B_z \rangle_T \hat{\mathbf{z}}$ with $\langle B_x \rangle_T \hat{\mathbf{x}} = \langle B_y \rangle_T \hat{\mathbf{y}} = 0$, we can estimate the average electric field as

$$\langle \mathbf{E} \rangle_T = -\frac{1}{c} \langle \mathbf{v} \rangle_T \times \langle \mathbf{B} \rangle_T. \tag{2}$$

With this prescription the mean electric field reduces to

$$\langle E_x \rangle_T = -\langle v_y \rangle_T \langle B_z \rangle_T / c \quad \langle E_y \rangle_T = \langle v_x \rangle_T \langle B_z \rangle_T / c \quad \langle E_z \rangle_T = 0. \tag{3}$$

In using the relations 3 the vertical magnetic field can be evaluated directly from the magnetogram time series and the horizontal velocity field provided by the FLCT technique. In the next section we will discuss the assumption of vertical average magnetic field in the quiet Sun and its evaluation via the magnetogram time series.

The current density that represents the source, at photospheric heights, of the observed magnetic field can be inferred from the Ampere's law that in cgs-Gaussian units reads

$$\nabla \times \mathbf{B} = \frac{4\pi}{c} \mathbf{J}, \tag{4}$$

where we have neglected the displacement current. Under the hypothesis of vertical magnetic field when averaging on supergranular time scales Equation 4 gives the solution

$$\langle J_x \rangle_T = \frac{c}{4\pi} \frac{\partial \langle B_z \rangle_T}{\partial y} \quad \langle J_y \rangle_T = -\frac{c}{4\pi} \frac{\partial \langle B_z \rangle_T}{\partial x} \quad \langle J_z \rangle_T = 0. \tag{5}$$

The energy conservation in a plasma volume in presence of electric and magnetic fields is expressed by the Poynting theorem, which states the relation between the energy density stored into an electromagnetic field, u, the energy flux quantified by the Poynting vector, $\mathbf{S}$, and the work done by the fields on a charge distribution. In differential form and for the case $\sigma \to \infty$ it is written

$$-\frac{\partial u}{\partial t} = \nabla \cdot \mathbf{S} + \mathbf{J} \cdot \mathbf{E}, \tag{6}$$

where $u = B^2/8\pi$ is the (magnetic) field energy per unit volume, $\mathbf{S} = \frac{c}{4\pi} \mathbf{E} \times \mathbf{B}$ is the Poynting vector representing the field energy flux, and $w \equiv \mathbf{J} \cdot \mathbf{E}$ is the rate of change of plasma mechanical energy per unit volume. Thus, knowing the average photospheric electric and magnetic fields and the current density on supergraular scales, it is possible to estimate the right hand side of Equation 6 and consequently the average rate of change of field energy per unit volume on the supergranular time scale T, namely $\langle \Delta U \rangle_T$. In particular, we obtain

$$\langle S_x \rangle_T = \frac{c}{4\pi} \langle E_y \rangle_T \langle B_z \rangle_T \quad \langle S_y \rangle_T = -\frac{c}{4\pi} \langle E_x \rangle_T \langle B_z \rangle_T \quad \langle S_z \rangle_T = 0, \tag{7}$$

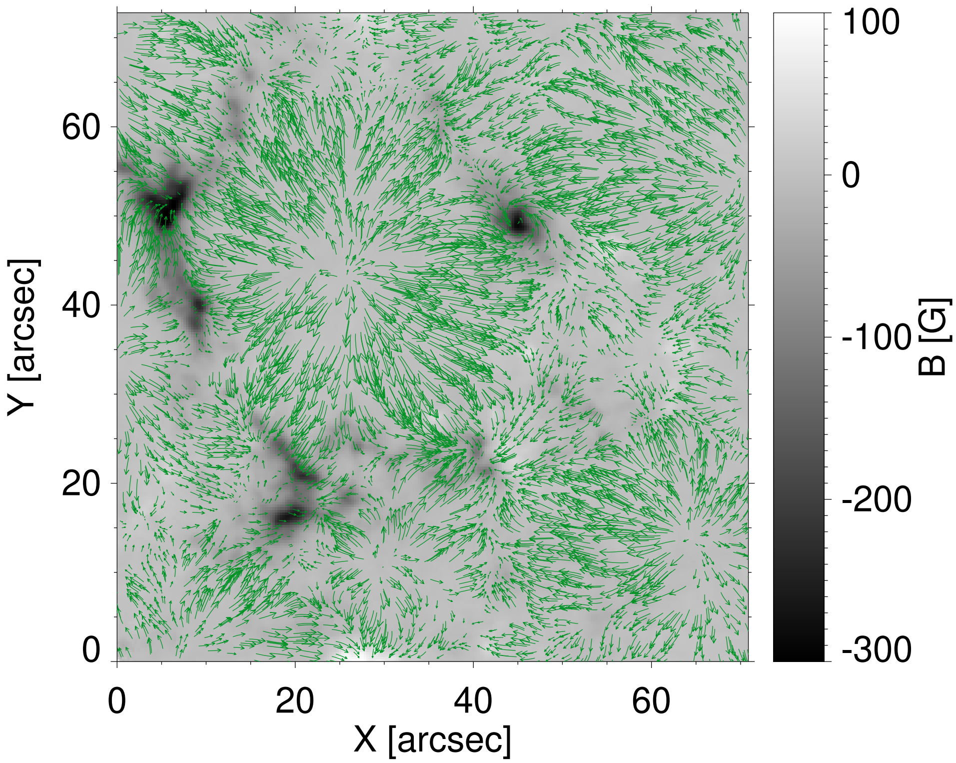

Figure 1. 24 hr-averaged magnetogram of the FoV saturated between −300 and 100 G. The boundaries of a supergranular cell are visible as enhancements of negative (black) field strengths. The green arrows represent the horizontal velocity field as computed with the FLCT method (see the text).

for $\langle \mathbf{S} \rangle_T$, which in this case is parallel to $\mathbf{v}$, and

$$\langle w \rangle_T = \langle J_x \rangle_T \langle E_x \rangle_T + \langle J_y \rangle_T \langle E_y \rangle_T, \tag{8}$$

for $\langle w \rangle_T$, respectively.

3. RESULTS AND DISCUSSION

3.1. *Electric field and current density*

We computed the photospheric electric field in the FoV under the hypothesis of very high Reynolds numbers and vertical magnetic field over the whole duration $T \simeq 24$ hr of observation by using Equations 3. The computed mean electric field is shown in the upper panel of Figure 2. In that figure, the electric field strength (saturated between $5 \cdot 10^{-5}$ and $3 \cdot 10^{-4}$ statvolt/cm) is represented in grey scale, while its direction is represented with golden arrows. As expected, the photospheric electric field is enhanced (and about one order of magnitude higher) in the boundaries of the supergranular cell, where the magnetic network is located (Giannattasio et al. 2014b), and the horizontal velocity is close to its maximum (Simon & Weiss 1989; Orozco Suárez et al. 2012; Giannattasio et al. 2014b). Due to the mutual directions of $\mathbf{v_h}$ and $\mathbf{B}$ the electric field in the network regions either crosses the magnetic field concentrations (see for example the region in the FoV at $X \in [0"; 10"]$ and $Y \in [35"; 55"]$), or departs radially from them (see for example the region of the FoV at $X \in [40"; 50"]$ and $Y \in [45"; 55"]$). As we can see in the horizontal velocity map shown in Figure 1 at the same locations, the former topology is associated with a plasma motion parallel to the supergranular cell boundary and towards increasing Y, while the latter is associated with a counterclockwise whirling motion already detected in previous works (Bonet et al. 2008, 2010; Shelyag et al. 2011; Chian et al. 2019) with a characteristic size of $\lesssim 5"$, corresponding to $\lesssim 3.6$ Mm on the photosphere.

We evaluated the mean current density in the FoV, namely $\langle \mathbf{J} \rangle_T$, by computing the components of Equation 5. The results are shown in the lower panel of Figure 2, where the current density strength (saturated between $2,000$ and $10,000$ statampere/cm^2) is represented in grey scale and its direction with white arrows. As expected, the current density strength is enhanced in correspondence with the magnetic network, and the shape of the current density field is such to encircle the magnetic field concentrations. It is interesting to notice

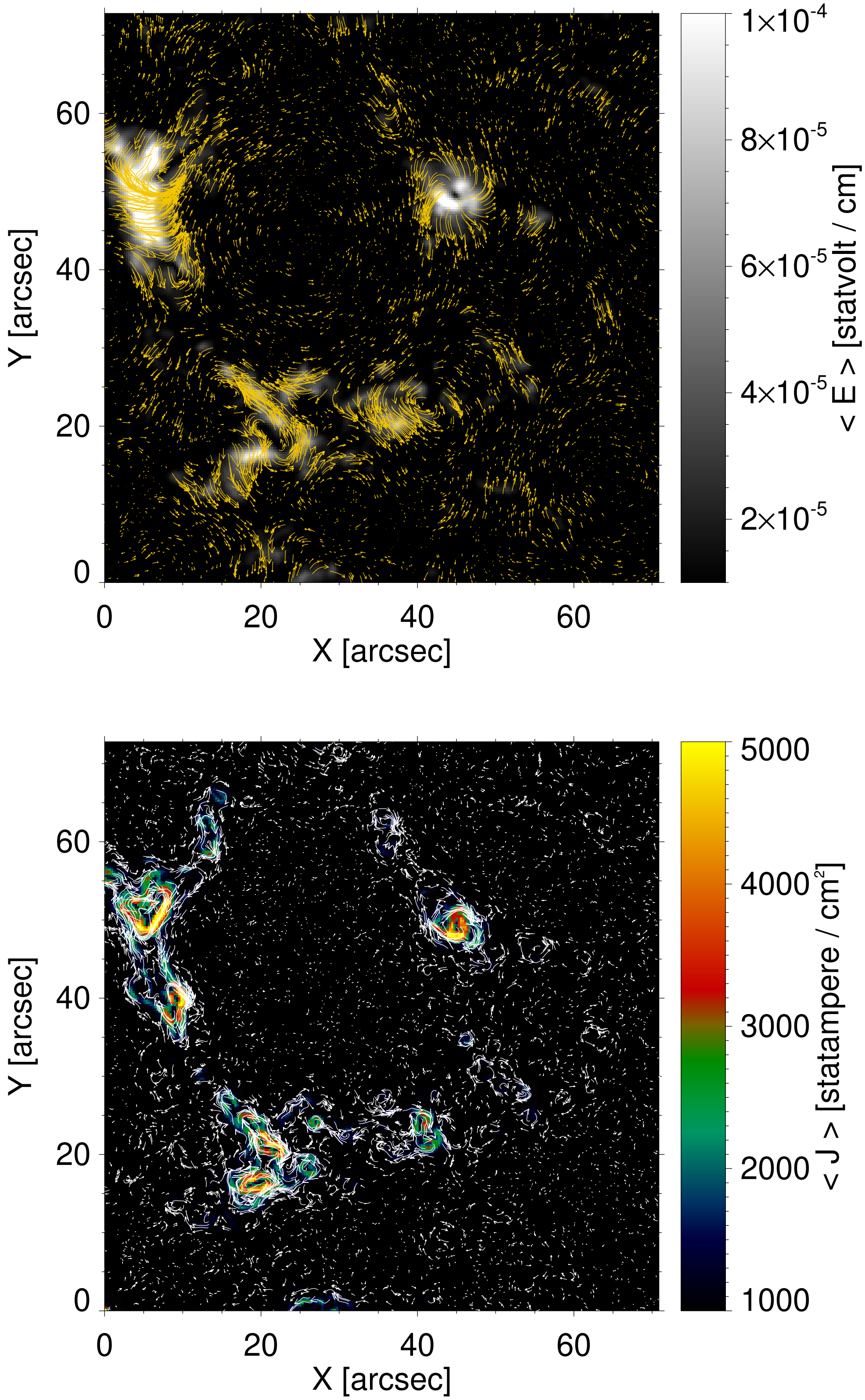

Figure 2. *Upper panel:* Mean electric field computed from Equations 3. The grey scale encodes the field strength, while the golden arrows show the direction of the electric field. *Lower Panel:* Mean current density computed from Equations 5. The colour encode the strength, while the white arrows show the direction of the current density.

the appearance of current density features that seem to exhibit a hierarchy of vortexes, with the biggest sizes around the strongest magnetic fields and a cascade down to smaller-sized features in the surroundings. This is visible especially in those regions at $Y \lesssim 40"$. In most models of turbulence, vortexes play a fundamental role, as represent a mechanism able to continuously transfer energy from the largest to the smallest scales, down to the dissipation ones (Frisch 1995). However, the turbulent nature of the current density features emerging in the FoV used will be investigated in a future work.

We underline that the mean electric field and current density were computed under the assumption that the average horizontal component of the magnetic field can be neglected compared to the vertical component, which was estimated by considering the magnetogram time series. This allowed us to use the relations 3 and 5. The question arises: Is this assumption reasonable? The magnetic field inclination in the quiet Sun at photospheric heights is still a debated topic, and in the last decades several works proposed controversial arguments to assert the dominance of vertical fields over horizontal ones or vice versa (see, e.g., Stenflo 2013a; Jafarzadeh et al. 2014; Borrero et al. 2017; Kianfar et al. 2018; Bellot Rubio & Orozco Suárez 2019, and references therein). No definitive conclusion to this debate was reached because of biases in observations and/or methods used to investigate this topic (Jafarzadeh et al. 2014). However, in this work we take advantage of an unprecedented 24-hr long magnetogram time series containing a supergranule. Over these spatial and temporal scales horizontal field components, which typically take place in the internetwork, are expected to average out, making their contribution to the mean magnetic field negligible respect to that of vertical fields. In fact, it is well known that the magnetic field in the quiet Sun is ubiquitous and quasi-isotropically distributed (Martin 1988; Meunier et al. 1998; Lites 2002; Harvey et al. 2007; López Ariste & Sainz Dalda 2012). The histograms of magnetic field inclination and azimuth are consistent with an isotropic distribution of transverse field associated with the weakest fields and the presence of kilo-Gauss fields that tend to be vertical (Stenflo 1982; Schüssler 1986; Orozco Suárez et al. 2007; Martínez González et al. 2008; Ishikawa & Tsuneta 2009; Bommier et al. 2009; Asensio Ramos 2009; Stenflo 2013b). An observational evidence of the isotropic distribution of magnetic field orientations is, for instance, the lack of Hanle rotation when performing inversions of spectropolarimetric data (see, e.g., Bommier et al. 2005; Ishikawa et al. 2008; Ishikawa & Tsuneta 2009, 2010; Bellot Rubio & Orozco Suárez 2019, and references therein). In fact, in the last decades the improvements in the inversion techniques allowed to show that the azimuth PDFs are nearly flat in the IN, indicating a random distribution of orientations of the transverse field component.

Deviations from these values are only observed in sunspots regions or for short time intervals. This is not the case of the present work. Thus, on supergranular scales many generations of shorter-living and arch-shaped bipolar magnetic fields are expected to emerge and evolve in the internetwork with randomly oriented horizonthal components; while vertical fields are expected to survive, especially in the network and in the nearby regions, where higher occurrences and longer decorrelation times are observed (Welsch et al. 2012; Giannattasio et al. 2018). Thus, the assumption that the photospheric magnetic field in the quiet Sun is mainly vertical on supegranular scales is reasonable. Under the additional hypothesis that in the observed FoV the magnetic filling factors are $ff = 1$ (Giannattasio et al. 2013), the magnetogram time series used in this work provides a reliable estimation for $\langle \mathbf{B} \rangle_T \simeq \langle B_z \rangle_T \hat{\mathbf{z}}$.

3.2. *Superdiffusion and the time scales of supergranulation*

Let us now consider the magneto-hydrodynamics (MHD) induction equation describing the rate of change of the magnetic field in a plasma volume. It reads

$$\frac{\partial \mathbf{B}}{\partial t} = \nabla \times (\mathbf{v} \times \mathbf{B}) + D_m \nabla^2 \mathbf{B}, \tag{9}$$

where $D_m = c^2/4\pi\sigma$ is the magnetic diffusivity. As it is well known, this equation describes the variation of the magnetic field in terms of advection (first term in the right-hand side, RHS) and diffusion (second term in the RHS) by and across the plasma flow, respectively. Under the ideal MHD hypothesis of magnetic field passively transported by the plasma flow (see, e.g., Giannattasio et al. 2013; Abramenko 2017) the diffusion term vanishes as $\sigma \to \infty$, and the magnetic field may be treated like a passive scalar having no influence on the dynamics of the surrounding plasma. It becomes a tracer helpful to depict the behaviour of the underneath plasma velocity. By abuse of notation we can keep this term in order to incorporate the (super-) diffusive properties of photospheric magnetic fields passively transported on supegranular scales by the underneath velocity field, which is structured in a wide range of scales due to turbulent convection (Berrilli et al. 2013, 2014; Giannattasio et al. 2019), and substitute D_m with the diffusivity D attributed to the spatially- and temporally- structured plasma velocity field and computed, e.g., in Giannattasio et al. (2013, 2014b). On the other hand, the ideal assumption is well fulfilled in the internetwork regions (inside the supergranule) but is less valid in the network regions, where the magnetic field may be strong (and thick) enough to exert a not negligible magnetic pressure on the surrounding plasma and resist the dragging of the velocity field. In fact, while for MEs with field strength below the equipartition value (Petrovay 1994; Giannattasio et al. 2013) the drag force determines the motion and the ME transport is passive, in the opposite case of field strengths above the equipartition value (which occurs in ~4% of the magnetic fields in the FoV, Giannattasio et al. 2013) MEs may move more independently of the surrounding plasma velocity and be less effective in passively tracing its behavior (Petrovay 1994). In this regime of, let's say, *resistively transported* magnetic field the penetration of plasma across magnetic field may occur, and tracking magnetic elements may probe a mix of dynamic properties from both the underneath velocity field and the magnetic field diffusing across plasma. It is thus interesting to estimate the magnitude of D relative to the pure advection term and the time scale of evolution of the magnetic field. To this aim, we can rewrite Equation 9 in an "order-of-magnitude" form to highlight the characteristic spatial and temporal scales at work. The magnetic field variation time, τ, on supergranular scales, l, can be evaluated by rewriting Equation 9 as

$$\frac{B}{\tau} \sim \frac{vB}{l} + D\frac{B}{l^2}. \qquad (10)$$

On supergranular scales $l \sim 3 \cdot 10^9$ cm, $v \sim 5 \cdot 10^4$ cm/s (Giannattasio et al. 2014b), $D \sim 4 \cdot 10^{12}$ cm^2/s at maximum (Giannattasio et al. 2013). The ratio between the advection to diffusion terms is $lv/D \sim 25$ on supergranular scales, meaning that the latter is at most $\sim 4\%$ of the former. From Equation 10 it follows that

$$\tau \sim \frac{l^2}{lv + D} \sim \frac{10^{19}}{10^{14} + 4 \cdot 10^{12}} \sim 10^5 s, \qquad (11)$$

or, in other words, $\tau \sim 28$ hr. Firstly, it emerges that even by considering the maximum superdiffusive term D measured by Giannattasio et al. (2013) in the network regions (i.e. in *resistively* transported magnetic field regime), it is negligible in the computation of τ as it gives a contribution of at most 4% of that from the advection term and represents only a small correction. This is, again, consistent with the hypothesis of diverging conductivity in the framework of ideal MHD, which remains a good approximation even within the network, where whatever the dynamics is, it deviates only slightly ($\sim 4\%$) from the ideal case $D = 0$. Secondly, due to this small D/lv ratio, the time scale of magnetic field variation on supergranular scales can be computed neglecting diffusion and is fully consistent with the typical lifetime of supergranules.

3.3. *The energy balance and the time scales of energy exchange*

In a recent work, Giannattasio et al. (2018) showed that the decorrelation time of magnetic field in the same FoV, t_D, which is the time after which the autocorrelation function of pixel-by-pixel magnetogram signal drops to $1/e$, is between ~ 0.5 and ~ 4 hr in the supergranular boundaries. This means that the magnetic field on supergranular scales decorrelates well before the decay time τ, and it is not sufficient to consider only the evolution of the magnetic field due to the underneath velocity field in order to explain the much faster decorrelation $t_d < \tau$. We have to consider also the energy that the magnetised plasma exchanges with the surroundings. In fact, both the incoming and outgoing energy flows to/from any plasma volume element may increase/decrease the local energy budget and result in a modification of the magnetic flux content and its consequent decorrelation. Such a local energetic balance is described by the Poynting Theorem (Equation 6). The simultaneous knowledge of $\langle \mathbf{E} \rangle_T$, $\langle \mathbf{J} \rangle_T$ and $\langle Bz \rangle_T$ allowed us to estimate the RHS of Equation 6 averaged on supergranular time scales. In that equation, the first term in RHS characterizes the energy flux that can be eventually carried by an electromagnetic field and propagate through a plasma volume element, i.e. the Poynting flux, and $div(\mathbf{S}) > 0$ corresponds to an outflow of energy from the plasma volume element, while $div(\mathbf{S}) < 0$ corresponds to an inflow of energy in the same volume element. The second term of RHS, w, has the dimension of a power per unit volume and provides an estimate of the rate at which the Lorentz force does work on the surrounding plasma causing an increase or decrease of the magnetic energy, u. In fact, by dotting the Lorentz force per unit volume, namely $\mathbf{f} = \rho\mathbf{E} + \mathbf{J} \times \mathbf{B}$, by the plasma velocity $\mathbf{v}$ we obtain

$$\mathbf{f} \cdot \mathbf{v} = \mathbf{J} \cdot \mathbf{E} = w, \qquad (12)$$

being the magnetic $\mathbf{J} \times \mathbf{B}$ term orthogonal to the velocity $\mathbf{v}$. Thus, only the electric field term of the Lorentz force does work on the surrounding plasma. In particular, a positive variation, $w > 0$, corresponds to a mechanical work done by the fields on the surrounding plasma, the more aligned currents and the electric field are, the greater the amount of energy transferred to the surrounding plasma. On the contrary, a negative variation, $w < 0$, corresponds to an increase of internal energy as the Lorentz force does work in the opposite direction, being directed against the electric field from the surrounding plasma to the plasma volume element under consideration. The critical values $div(\mathbf{S}) = 0$ and $w = 0$ correspond, respectively, to a balance between the inflowing/outflowing electromagnetic energy through the volume element and a null exchange of energy with the surrounding plasma. In the upper panel of Figure 3 we show the time-averaged rate of change of mechanical energy per unit volume, w, saturated between -0.2 and 0.2 erg $\mathrm{cm}^{-3}\mathrm{s}^{-1}$ and attributed to the Lorenz force acting on current density via the electric field. The quantity w ranges between -0.92 and 0.27 erg/cm^{3}s. In correspondence of the supergranular boundaries there is an enhancement of this quantity in absolute value, such that the appearing features are quite symmetrically divided into adjacent sub-regions with opposite sign (blue/red for negative/positive, respectively). This is consistent with the coexistence of nearby regions where, on average, energy is lost (gained) due to the positive (negative) work done by the Lorenz force per unit volume, the sign being driven by the mutual directions of vectors $\mathbf{J}$ and $\mathbf{E}$. In these promiscuous regions the observed transition between positive and negative values of w occurs in the center, where $w = 0$. The only way to satisfy this condition is that the current density and the electric field are mutually orthogonal, as on average neither the former nor the latter are null.

In the lower panel of Figure 3 we show the time-averaged variation of the divergence of the Poynting vector, $div(\mathbf{S})$ that should be associated with an electromagnetic energy flow saturated between -0.8 and 0.8 erg $\mathrm{cm}^{-3}\mathrm{s}^{-1}$. The quantity $div(\mathbf{S})$ ranges between -1.23 and 1.59 erg/cm^{3}s. Also in this case, in correspondence of the supergranular boundaries there is an enhancement of this quantity in absolute value, which appears to be symmetrically divided into adjacent subregions with opposite sign. This implies the coexistence of nearby regions where, on average, energy is lost (gained) due to the positive (negative) energy flux, the sign being driven by the mutual directions of vectors $\mathbf{B}$ and $\mathbf{E}$. In these promiscuous regions the observed transition between positive and negative values of $div(\mathbf{S})$ occurs, again, in the centre, where $div(\mathbf{S}) = 0$. The only way to satisfy this condition is that the magnetic and electric fields are parallel, as on average neither the former nor the latter are null. We note that the two RHS terms in Equation 6 are of the same order of magnitude, thus both contribute with the same weight to the estimation of the energy density variation averaged on supergranular scales, namely $\langle \Delta u \rangle_T$.

The timescale, τ^*, associated with the energy variation of a plasma volume element on supergranular scales can be computed by rewriting Equation 6 as follows:

$$\frac{u}{\tau^*} \sim JE + \frac{S}{l}. \tag{13}$$

By assuming $u \simeq B^2/8\pi$ with $B \sim 300$ G as a typical value for the magnetic field in the FoV (Giannattasio et al. 2013), considering the supergranular length scale $l \sim 3 \cdot 10^9$ cm like did above, and once computed the Poynting vector $S \sim 10^8$ erg/cm^{2}s we evaluated the time scale of energy exchange

$$\tau^* \sim \frac{B^2 l}{8\pi(JEl + S)} \sim \frac{9 \cdot 10^4 \cdot 3 \cdot 10^9}{8 \cdot 3 \cdot (5 \cdot 10^3 \cdot 10^{-4} \cdot 3 \cdot 10^9 + 10^8)} \sim 10^4 s, \tag{14}$$

which corresponds to $\tau^* \sim 2.8$ hr. This time scale is of the same order of magnitude of the magnetic field decorrelation times observed in the same FoV by Giannattasio et al. (2018). This suggests that the energy balance due to the interaction of plasma with both photospheric electric and magnetic fields on supergranular scales plays a crucial role in modifying the magnetic patterns that characterize the photospheric supergranulation. In order to show this, in Figure 4 we show the averaged LHS of Equation 6, $\langle \Delta u \rangle$ on supergranular scales saturated between -1.5 and 1.5 erg/cm^{3}s. The quantity $\langle \Delta u \rangle$ ranges between -1.76 and 2.08 erg/cm^{3}s. In that figure, we superposed in green contour plots of the magnetic decorrelation times $t_D > 120$ min computed in Giannattasio et al. (2018). As we can see, the longer t_D times occur mostly where $\langle \Delta u \rangle \geq 0$, i.e. where the average energy variation is null or moderately positive. This means that magnetic field decorrelates at longer times mainly where the energy variation is null (in a stationary situation), as we may expect, or the energy slightly increases, as this energy supply is effective in contrasting the field decay and the consequent decorrelation. The only exception is represented by the vortex motion observed in the region of the FoV at $X \in [40"; 50"]$ and $Y \in [45"; 55"]$, within which we have basically $\langle \Delta u \rangle \sim 0$, and only a few very small sub-areas in the centre are associated with longer t_D times. As found by Giannattasio et al. (2018) this region is characterised by a very high magnetic field occurrence (near 100%) and $40 \lesssim t_D \lesssim 50$ min, which is probably due to the presence of different and tightly packed magnetic elements moving in a very restricted area. Thus, the lack of magnetic fields with long t_D times in this region with $\langle \Delta u \rangle = 0$ is consistent with the presence of an intense vortex that may act as an attractor constraining the dynamics of the nearby magnetic elements to evolve in a very restricted area and causing these magnetic elements to pile up there. We can interpret these results by depicting the following simple scenario. Turbulent convection produces mag-

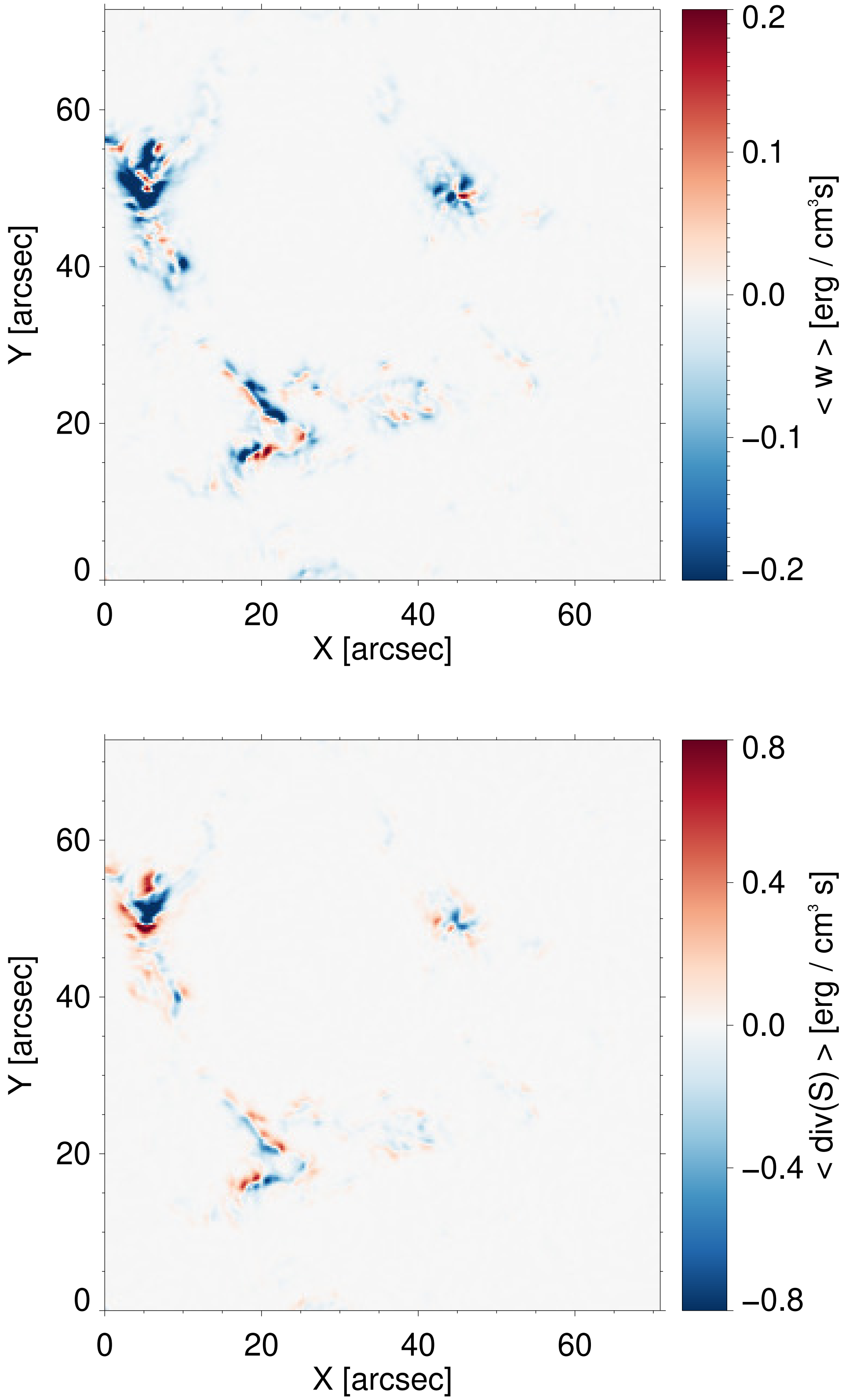

Figure 3. *Upper panel:* Mean energy variation rate, w, due to the Lorentz force. *Lower panel:* Mean divergence of the Poynting vector, i.e. the electromagnetic field energy flux available in the plasma volume element.

netic fields and drives their motion in the solar photosphere at all scales, from sub-granular to supergranular.

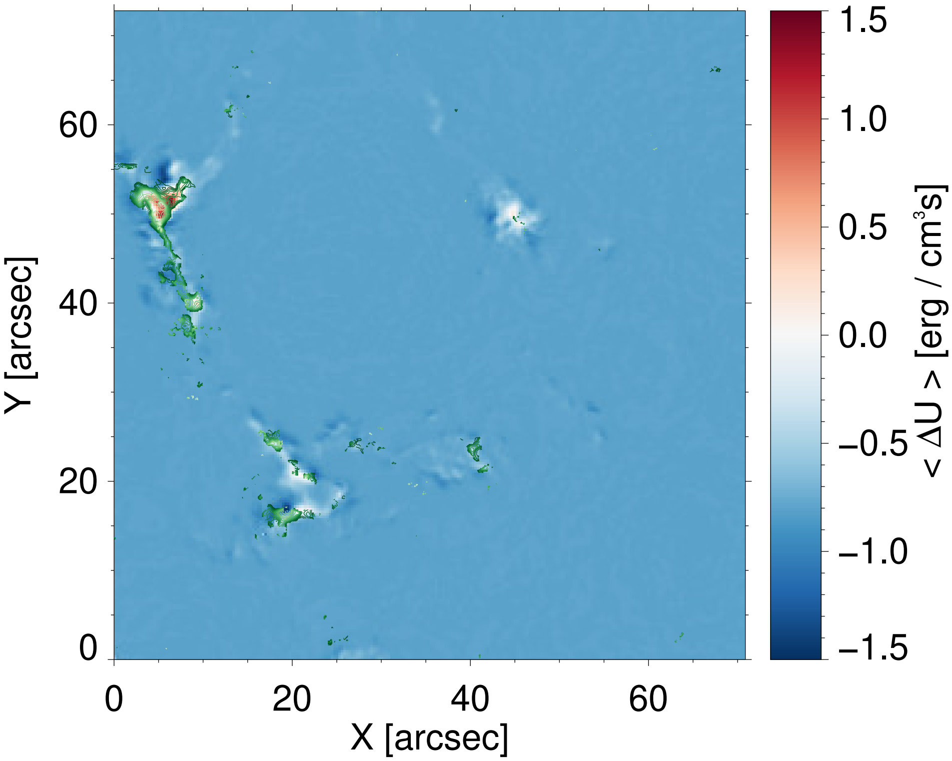

Figure 4. Mean energy variation rate, $\langle \Delta u \rangle$ saturated between -1.5 and 1.5 erg/cm^{3}s. The superposed green lines are contour plots of the magnetic decorrelation times $t_D > 120$ min computed in Giannattasio et al. (2018) (see the text).

The coupling between photospheric plasma flows and magnetic fields contributes to the generation of electric fields. The interaction between electric and magnetic fields and plasma currents may alter the local energy content of plasma via, e.g., the Lorentz force and the energy flux flowing through adjacent plasma volumes. For example, a positive work done by the Lorentz force, $w > 0$, accelerates the surrounding plasma in direction of the flows and can, in principle, enhance the currents, while a simultaneous decrease of local energy u occurs. On the contrary, a negative work, $w < 0$, transfers energy to the plasma element causing an increase of u. The same applies to the flux of energy associated with electric and magnetic fields, namely $div(\mathbf{S})$, as an outgoing (incoming) energy from (to) the plasma element corresponds to a decrease (increase) of u. What is important is the balance given by the sum of these two contributions, and it appears clear the correlation between longer magnetic field decorrelation times, t_D, and the regions where $\langle \Delta u \rangle \geq 0$. Moreover, when considering the energy balance given by the Poynting theorem, the time scale τ^* on which the magnetic energy density varies is consistent with the decorrelation time of the magnetic field. In particular, τ^* is not long enough to cause, for example, the decay of the supergranule, which must be sustained by both the enhancement of currents and an energy flux coming from the nearby regions, in form, for example, of turbulent transport.

4. SUMMARY AND CONCLUSIONS

Magnetic elements (MEs) are ubiquitous in the quiet photosphere. Studying their dynamic properties may help to shed light on both the mechanisms of storage and transfer of energy to the upper atmospheric layers, and the dynamic properties of the photospheric turbulent velocity field under the hypothesis that MEs are passively transported by the plasma flow. The knowledge of the electric field and current density together with the magnetic field, allows to estimate the energy balance in the photosphere via the Poynting theorem, which links the rate of variation of the energy density in a plasma volume element with the work done by the electric field on the surrounding plasma and the energy flux flowing through the volume element. However, the computation of local electric field at any time requires the knowledge, for example, of the vector magnetic field, which can be obtained only via the inversion of spectropolarimetric (SP) full-Stokes data. On the other hand, it is not possible to acquire long SP data targeted at large FoVs with fast cadence and high spectropolarimetric sensitivity, since this experimental setup has the result of reducing the number of spectral points sampled, which affects the goodness of results, and vice versa. Despite of this, we can still obtain a reasonable approximation for the electric field averaged on supergranular scales by using only magnetogram time series instead of full-Stokes data. Our findings may be itemized as follows:

1. For the first time we provided average photospheric electric field and current density in the quiet Sun on supergranular scales by using a ∼24 hr-long magnetogram time series enclosing an entire supergranule;

2. By applying the Poynting theorem we computed the average rate of change of field energy per unit volume on supergranular scales, $\langle \Delta u \rangle$, and found that the timescale associated with the energy variation is consistent with the magnetic field decorrelation times, t_D, in the same FoV retrieved in Giannattasio et al. (2018);

3. The longer t_D times are co-spatial with the regions where $\langle \Delta u \rangle \geq 0$, indicating that the energy supply effectively balances the magnetic field and energy decay.

We regard that this study could represent a turning point for the exploitation of long magnetogram time series to investigate more comprehensively the energy balance at large and long scales. Due to the huge amount of magnetic flux emerging in the quiet Sun, this energy should give a fundamental contribution to sustain the upper atmospheric layers.

ACKNOWLEDGMENTS

This work is supported by tne Italian MIUR-PRIN grant 2017APKP7T on *Circumterrestrial Environment: Impact of Sun-Earth Interaction*. FG is grateful to M. Gošić and L. Bellot Rubio for providing the data here analyzed. This paper is based on data acquired in the framework of the Hinode Operation Plan 151 entitled "Flux replacement in the network and internetwork". Hinode is a Japanese mission developed and launched by ISAS/JAXA, collaborating with NAOJ as a domestic partner, NASA and STFC (UK) as international partners. Scientific operation of the Hinode mission is conducted by the Hinode science team organized at ISAS/JAXA. This team mainly consists of scientists from institutes in the partner countries. Support for the post-launch operation is provided by JAXA and NAOJ (Japan), STFC (U.K.), NASA, ESA, and NSC (Norway).

REFERENCES

Abramenko, V. I. 2017, MNRAS, 471, 3871, doi: 10.1093/mnras/stx1880

Asensio Ramos, A. 2009, ApJ, 701, 1032, doi: 10.1088/0004-637X/701/2/1032

Bellot Rubio, L., & Orozco Suárez, D. 2019, Living Reviews in Solar Physics, 16, 1, doi: 10.1007/s41116-018-0017-1

Berrilli, F., Scardigli, S., & Del Moro, D. 2014, A&A, 568, A102, doi: 10.1051/0004-6361/201424026

Berrilli, F., Scardigli, S., & Giordano, S. 2013, SoPh, 282, 379, doi: 10.1007/s11207-012-0179-2

Bommier, V., Derouich, M., Landi Degl'Innocenti, E., Molodij, G., & Sahal-Bréchot, S. 2005, A&A, 432, 295, doi: 10.1051/0004-6361:20035773

Bommier, V., Martínez González, M., Bianda, M., et al. 2009, A&A, 506, 1415, doi: 10.1051/0004-6361/200811373

Bonet, J. A., Márquez, I., Sánchez Almeida, J., Cabello, I., & Domingo, V. 2008, ApJL, 687, L131, doi: 10.1086/593329

Bonet, J. A., Márquez, I., Sánchez Almeida, J., et al. 2010, ApJL, 723, L139, doi: 10.1088/2041-8205/723/2/L139

Borrero, J. M., Jafarzadeh, S., Schüssler, M., & Solanki, S. K. 2017, SSRv, 210, 275, doi: 10.1007/s11214-015-0204-5

Cattaneo, F., Emonet, T., & Weiss, N. 2003, ApJ, 588, 1183, doi: 10.1086/374313

Chae, J. 1999, in Astronomical Society of the Pacific Conference Series, Vol. 183, High Resolution Solar Physics: Theory, Observations, and Techniques, ed. T. R. Rimmele, K. S. Balasubramaniam, & R. R. Radick, 375

Chae, J., & Sakurai, T. 2008, ApJ, 689, 593, doi: 10.1086/592761

Chian, A. C. L., Silva, S. S. A., Rempel, E. L., et al. 2019, MNRAS, 488, 3076, doi: 10.1093/mnras/stz1909

Davis, W. D. 1977, SoPh, 54, 139, doi: 10.1007/BF00146430

Del Moro, D., Berrilli, F., Duvall, T. L., J., & Kosovichev, A. G. 2004, SoPh, 221, 23, doi: 10.1023/B:SOLA.0000033363.15641.8f

Démoulin, P., & Berger, M. A. 2003, SoPh, 215, 203, doi: 10.1023/A:1025679813955

Fisher, G. H., & Welsch, B. 2007, in American Astronomical Society Meeting Abstracts, Vol. 210, American Astronomical Society Meeting Abstracts #210, 92.11

Fisher, G. H., & Welsch, B. T. 2008, in Astronomical Society of the Pacific Conference Series, Vol. 383, Subsurface and Atmospheric Influences on Solar Activity, ed. R. Howe, R. W. Komm, K. S. Balasubramaniam, & G. J. D. Petrie, 373. https://arxiv.org/abs/0712.4289

Fisher, G. H., Welsch, B. T., Abbett, W. P., & Bercik, D. J. 2010, ApJ, 715, 242, doi: 10.1088/0004-637X/715/1/242

Frisch, U. 1995, Turbulence (Cambridge university press)

Giannattasio, F., Berrilli, F., Biferale, L., et al. 2014a, A&A, 569, A121, doi: 10.1051/0004-6361/201424380

Giannattasio, F., Berrilli, F., Consolini, G., et al. 2018, A&A, 611, A56, doi: 10.1051/0004-6361/201730583

Giannattasio, F., Consolini, G., Berrilli, F., & Del Moro, D. 2019, ApJ, 878, 33, doi: 10.3847/1538-4357/ab1be2

Giannattasio, F., Del Moro, D., Berrilli, F., et al. 2013, ApJL, 770, L36, doi: 10.1088/2041-8205/770/2/L36

Giannattasio, F., Stangalini, M., Berrilli, F., Del Moro, D., & Bellot Rubio, L. 2014b, ApJ, 788, 137, doi: 10.1088/0004-637X/788/2/137

Gošić, M., Bellot Rubio, L. R., del Toro Iniesta, J. C., Orozco Suárez, D., & Katsukawa, Y. 2016, ApJ, 820, 35, doi: 10.3847/0004-637X/820/1/35

Gošić, M., Bellot Rubio, L. R., Orozco Suárez, D., Katsukawa, Y., & del Toro Iniesta, J. C. 2014, ApJ, 797, 49, doi: 10.1088/0004-637X/797/1/49

Gošić, M., de la Cruz Rodríguez, J., De Pontieu, B., et al. 2018, ApJ, 857, 48, doi: 10.3847/1538-4357/aab1f0

Hahn, M., & Savin, D. W. 2014, ApJ, 795, 111, doi: 10.1088/0004-637X/795/2/111

Harvey, J. W., Branston, D., Henney, C. J., Keller, C. U., & SOLIS and GONG Teams. 2007, ApJL, 659, L177, doi: 10.1086/518036

Hirzberger, J. 2002, A&A, 392, 1105, doi: 10.1051/0004-6361:20020902

Hood, A. W., & Hughes, D. W. 2011, Physics of the Earth and Planetary Interiors, 187, 78, doi: 10.1016/j.pepi.2011.04.010

Ishikawa, R., & Tsuneta, S. 2009, A&A, 495, 607, doi: 10.1051/0004-6361:200810636

—. 2010, ApJL, 718, L171, doi: 10.1088/2041-8205/718/2/L171

Ishikawa, R., Tsuneta, S., Ichimoto, K., et al. 2008, A&A, 481, L25, doi: 10.1051/0004-6361:20079022

Jafarzadeh, S., Solanki, S. K., Lagg, A., et al. 2014, A&A, 569, A105, doi: 10.1051/0004-6361/201423414

Jefferies, S. M., Fleck, B., Murphy, N., & Berrilli, F. 2019, ApJL, 884, L8, doi: 10.3847/2041-8213/ab4719

Jordan, C., Bartoe, J. D. F., & Brueckner, G. E. 1980, ApJ, 240, 702, doi: 10.1086/158278

Kazachenko, M. D., Fisher, G. H., & Welsch, B. T. 2014, ApJ, 795, 17, doi: 10.1088/0004-637X/795/1/17

Kazachenko, M. D., Fisher, G. H., Welsch, B. T., Liu, Y., & Sun, X. 2015, ApJ, 811, 16, doi: 10.1088/0004-637X/811/1/16

Kianfar, S., Jafarzadeh, S., Mirtorabi, M. T., & Riethmüller, T. L. 2018, SoPh, 293, 123, doi: 10.1007/s11207-018-1341-2

Kosugi, T., Matsuzaki, K., Sakao, T., et al. 2007, SoPh, 243, 3, doi: 10.1007/s11207-007-9014-6

Kusano, K., Maeshiro, T., Yokoyama, T., & Sakurai, T. 2002, ApJ, 577, 501, doi: 10.1086/342171

Lites, B. W. 2002, ApJ, 573, 431, doi: 10.1086/340120

López Ariste, A., & Sainz Dalda, A. 2012, A&A, 540, A66, doi: 10.1051/0004-6361/201118191

Martin, S. F. 1988, SoPh, 117, 243, doi: 10.1007/BF00147246

Martínez González, M. J., Asensio Ramos, A., López Ariste, A., & Manso Sainz, R. 2008, A&A, 479, 229, doi: 10.1051/0004-6361:20078500

Meunier, N., Solanki, S. K., & Livingston, W. C. 1998, A&A, 331, 771

Moran, T., & Foukal, P. 1991, SoPh, 135, 179, doi: 10.1007/BF00146705

Orozco Suárez, D., Katsukawa, Y., & Bellot Rubio, L. R. 2012, ApJL, 758, L38, doi: 10.1088/2041-8205/758/2/L38

Orozco Suárez, D., Bellot Rubio, L. R., del Toro Iniesta, J. C., et al. 2007, ApJL, 670, L61, doi: 10.1086/524139

Parker, E. N. 1963, ApJ, 138, 552, doi: 10.1086/147663

Petrovay, K. 1994, in Solar Surface Magnetism, ed. R. J. Rutten & C. J. Schrijver (Dordrecht: Springer Netherlands), 415–440, doi: 10.1007/978-94-011-1188-1_35

Rajaguru, S. P., Sangeetha, C. R., & Tripathi, D. 2019, ApJ, 871, 155, doi: 10.3847/1538-4357/aaf883

Rast, M. P. 2003, ApJ, 597, 1200, doi: 10.1086/381221

Requerey, I. S., Cobo, B. R., Gošić, M., & Bellot Rubio, L. R. 2018, A&A, 610, A84, doi: 10.1051/0004-6361/201731842

Rieutord, M., Rincon, F., & Roudier, T. 2012, in EAS Publications Series, Vol. 55, EAS Publications Series, ed. M. Faurobert, C. Fang, & T. Corbard, 5–13, doi: 10.1051/eas/1255001

Rouppe van der Voort, L. H. M., Rutten, R. J., & Vissers, G. J. M. 2016, A&A, 592, A100, doi: 10.1051/0004-6361/201628889

Schuck, P. W. 2006, ApJ, 646, 1358, doi: 10.1086/505015

—. 2008, ApJ, 683, 1134, doi: 10.1086/589434

Schüssler, M. 1986, in Small Scale Magnetic Flux Concentrations in the Solar Photosphere, ed. W. Deinzer, M. Knölker, & H. H. Voigt, 103

Shelyag, S., Keys, P., Mathioudakis, M., & Keenan, F. P. 2011, A&A, 526, A5, doi: 10.1051/0004-6361/201015645

Simon, G. W., Title, A. M., & Weiss, N. O. 2001, ApJ, 561, 427, doi: 10.1086/322243

Simon, G. W., & Weiss, N. O. 1989, ApJ, 345, 1060, doi: 10.1086/167976

Stangalini, M., Giannattasio, F., & Jafarzadeh, S. 2015, A&A, 577, A17, doi: 10.1051/0004-6361/201425273

Stenflo, J. O. 1982, SoPh, 80, 209, doi: 10.1007/BF00147969

—. 2013a, A&A, 555, A132, doi: 10.1051/0004-6361/201321608

—. 2013b, A&A Rv, 21, 66, doi: 10.1007/s00159-013-0066-3

Trujillo Bueno, J., Shchukina, N., & Asensio Ramos, A. 2004, Nature, 430, 326, doi: 10.1038/nature02669

Tsuneta, S., Ichimoto, K., Katsukawa, Y., et al. 2008, SoPh, 249, 167, doi: 10.1007/s11207-008-9174-z

Viticchié, B., Del Moro, D., & Berrilli, F. 2006, ApJ, 652, 1734, doi: 10.1086/508332

Weiss, N. 2001, Astronomy and Geophysics, 42, 3.10, doi: 10.1046/j.1468-4004.2001.42310.x

Welsch, B. T., Fisher, G. H., Abbett, W. P., & Regnier, S. 2004, ApJ, 610, 1148, doi: 10.1086/421767

Welsch, B. T., Kusano, K., Yamamoto, T. T., & Muglach, K. 2012, ApJ, 747, 130, doi: 10.1088/0004-637X/747/2/130

Wien, W. 1916, Annalen der Physik, 354, 842, doi: 10.1002/andp.19163540704